



POTSDAM-INSTITUT FÜR
KLIMAFOLGENFORSCHUNG

Originally published as:

[Boers, N.](#), [Liu, T.](#), [Bathiany, S.](#), [Ben-Yami, M.](#), [Blaschke, L.](#), [Bochow, N.](#), Boulton, C. A., Lenton, T. M., [Morr, A.](#), [Nian, D.](#), Rypdal, M., Smith, T. (2025): Destabilization of Earth system tipping elements. - Nature Geoscience, 18, 949-960.

DOI: <https://doi.org/10.1038/s41561-025-01787-0>

Destabilization of Earth system tipping elements

Niklas Boers^{1,2,3,*,†}, Teng Liu^{1,2,4,*}, Sebastian Bathiany^{1,2}, Maya Ben-Yami^{1,2},
Lana L. Blaschke^{1,2}, Nils Bochow^{2,5}, Chris A. Boulton³, Timothy M.
Lenton³, Andreas Morr^{1,2}, Da Nian², Martin Rypdal⁵, Taylor Smith⁶

¹Earth System Modelling, School of Engineering and
Design, Technical University of Munich, Munich, Germany

²Potsdam Institute for Climate Impact Research, Potsdam, Germany

³Global Systems Institute, University of Exeter, Exeter, UK

⁴School of Systems Science, Beijing Normal University, Beijing, China

⁵Department of Mathematics and Statistics, Faculty of Science and
Technology, UiT The Arctic University of Norway, Tromsø, Norway

⁶Institute of Geosciences, Universität Potsdam, Potsdam, Germany

*These authors contributed equally to this work

†e-mail: n.boers@tum.de, boers@pik-potsdam.de

(Dated: June 30, 2025)

Abstract

16
17 There is rising concern that several parts of the Earth system might abruptly transition to alternative stable
18 states in response to anthropogenic climate and land-use change. Key candidates of such tipping elements
19 include the Greenland Ice Sheet, the Atlantic Meridional Overturning Circulation, the South American
20 monsoon system, and the Amazon rainforest. Due to their complex dynamics and feedbacks between them
21 via oceanic and atmospheric coupling, the levels of anthropogenic forcing at which transitions to alternative
22 states can be expected remain uncertain. Here, we demonstrate how such interactions can generate spurious
23 signals and potentially mask genuine signs of destabilization. We further review and present observation-
24 based evidence that the stability of these four tipping elements has declined in recent decades, suggesting
25 that they have moved toward their critical thresholds, which may be crossed within the range of unmitigated
26 anthropogenic warming. Our results call for better monitoring of these tipping elements and for increased
27 efforts to stop greenhouse gas emissions and land-use change.

28 I. INTRODUCTION

29 Different lines of empirical and modeling evidence suggest that several components of the Earth
30 system may respond nonlinearly to gradual changes in forcing and potentially transition abruptly
31 between alternative stable states [1–3]. The evidence mainly originates from paleoclimate proxy
32 records [4–6], and comprehensive climate model simulations [7–10]. Key examples of these tip-
33 ping elements include the Greenland and West Antarctic Ice Sheets (GrIS and WAIS), the Atlantic
34 Meridional Overturning Circulation (AMOC), the tropical monsoon systems including the South
35 American monsoon system (SAMS), and the Amazon rainforest (Fig. 1a). These subsystems are
36 coupled through oceanic and atmospheric circulation patterns, resulting in teleconnections among
37 them [11, 12]. When one subsystem undergoes a transition that alters the background state of an-
38 other subsystem, this can trigger a transition in the second subsystem as well [13]. Such dynamical
39 interactions, which lead to coupled transitions, are examples of “tipping cascades” [14], although
40 the couplings can have stabilizing effects as well [15]. Fig. 1b illustrates conceptual tipping ele-
41 ments under the influence of a linear global temperature increase. The coupling between tipping
42 elements, where the control parameter of one element depends on the state of the preceding ele-

43 ment, can result in a critical threshold of the subsequent element being crossed earlier or later than
44 without any coupling. Additionally, the complexity of tipping elements is also reflected in their dif-
45 fering characteristic timescales: the Amazon rainforest and the SAMS have timescales of decades,
46 the AMOC spans decades to a century, and typical GrIS timescales range from centuries to mil-
47 lennia. These timescale variations lead to distinct critical dynamics for each tipping element once
48 global warming (or deforestation for the case of the Amazon) exceeds a certain threshold [16, 17].
49 Predicting the future dynamics of these key tipping elements in response to further rising temper-
50 atures and environmental change is a primary challenge in current climate change research, with
51 strong implications for the global sociopolitical efforts to mitigate dangerous climate change [18].

52 Ideally, comprehensive Earth system models (ESMs) would predict the future dynamics of these
53 tipping elements. A systematic search revealed a number of abrupt transitions in simulations from
54 the fifth phase of the Climate Model Intercomparison Project (CMIP5), though the cases identi-
55 fied were often smaller in scale than regional tipping elements, and not robust across models [8].
56 There has been considerable progress in reproducing abrupt transitions evidenced in paleoclimate
57 records with comprehensive models in recent years [7, 10, 19]. This success demonstrates the
58 power of ESMs, yet important gaps remain: interactive ice sheets are still absent from many model
59 runs, and the representation of other tipping elements and their interactions remains incomplete.
60 Moreover, the global mean surface temperature, which is a key forcing for these tipping elements,
61 varies between models: state-of-the-art models, such as those from CMIP6, exhibit considerable
62 uncertainty in their temperature projections even for the same assumed greenhouse gas emission
63 pathway, mainly due to the large spread in the models' climate sensitivity [20, 21]. In addition,
64 several studies indicate that these models may have too stable a representation of some key tip-
65 ping elements [10, 22–25], given that it is difficult and, in some cases, not possible to reproduce
66 past abrupt climate changes using current models [9, 26]. For these reasons, the risk of tipping
67 and the critical temperature forcing levels for different tipping elements remain highly uncertain.
68 Although comprehensive ESMs will remain the most valuable tool for assessing the nature and im-
69 pacts of ongoing climate change, a more observation-based approach to studying tipping elements
70 can provide valuable complementary analysis.

71 An intuitive source of empirical evidence is to look at whether tipping elements are changing
72 state in an undesirable direction [3], e.g., the AMOC weakening [27, 28] or ice sheets losing

73 mass [29, 30]. However, changes in the mean state of nonlinear systems are rarely informative
74 about their stability. We consider stability as a system’s capacity to recover from perturbations;
75 technically, we define it in terms of the linear restoring rate λ , which is obtained by linearizing the
76 dynamics around a given stable equilibrium state and can be estimated from observational data.

77 We first review recent methodological advances to investigate and predict the dynamics of cou-
78 pled Earth system tipping elements in terms of dynamical system theory with a focus on bifurca-
79 tions, critical slowing down (CSD; Box 1), and the associated early-warning signals (EWS; Box
80 1) [31–33]. These methods have been extensively tested over the last two decades. For example, it
81 has been shown that EWS precede several past abrupt climate transitions, such as the Paleocene-
82 Eocene Thermal Maximum event 56 million years ago [34, 35], the Oligocene-Miocene Transition
83 23 million years ago [36] and terminations of several glacial intervals during the last one million
84 years [37, 38]. Moreover, the decadal-scale frequency bands of Greenland ice core records reveal
85 EWS for the so-called Dansgaard-Oeschger (DO) events, which are abrupt climate shifts during
86 the last glacial period likely associated with AMOC transitions [39–41]. Furthermore, detectable
87 EWS precede critical transitions in controlled, real-world experiments [42–44] and in model sim-
88 ulations of many different ecosystems and other components of the climate system [32, 45–47].
89 EWS have also been identified prior to forced tipping points in different model simulations, in-
90 cluding AMOC collapse in response to increasing CO₂ [48] or artificial freshwater hosing in the
91 North Atlantic [49, 50]. Recently, EWS have been identified in simulations of the marine ice
92 sheet instability in West Antarctica [51]. Such identification of EWS in modeled time series can
93 guide the search for EWS in observational records [52]. Moreover, the application of CSD to ob-
94 servational data has recently revealed the destabilization of components of the climate and Earth
95 system [53–58].

96 Here, we review and present evidence that four major interconnected tipping elements in the
97 Earth system, namely the GrIS, the AMOC, the Amazon, and the SAMS, are currently losing
98 stability, consistent with approaching critical transitions. We begin by reviewing the theory and
99 practical application of EWS based on CSD, and then highlight how interactions between tipping
100 elements can distort or obscure these signals, leading to potential false positives or missed warn-
101 ings, and how incorporating prior knowledge about system dynamics can help reduce such risk. We
102 then summarize and reinforce existing observation-based evidence showing the four elements’ loss

103 of stability, applying a consistent metric across elements to facilitate direct comparison. Finally,
104 we discuss the feedbacks coupling these four elements, how they affect the critical forcing levels
105 of the individual subsystems, and how they may influence EWS. We close by elaborating upon
106 previous suggestions [33, 59, 60] that a more comprehensive tipping element resilience sensing
107 system could make a valuable contribution to climate risk monitoring.

108 **ASSUMPTIONS, APPLICABILITY, AND CAVEATS**

109 Classical EWS, given by rising variance and autocorrelation (see Box 1), are technically lim-
110 ited despite their success in many applications. Several assumptions are made, sometimes implic-
111 itly [61]. One assumption is that the system state is not too far from equilibrium. Otherwise, the
112 linearization needed to establish a connection between the system's stability on the one hand, and
113 the variance and autocorrelation on the other hand (see Box 1), would not be a valid approximation.
114 Yet even for rate-induced transitions, where this assumption is not satisfied, rising variance and au-
115 tocorrelation can still serve as EWS for the transition, although delayed in that case [62]. Another
116 assumption stems from the most common model (see Eq. 1 in Box 1), which assumes that the noise
117 term is white, additive, and stationary. Several approaches to generalize to colored noise forcing
118 have recently been introduced [47, 63, 64]. In cases where the noise forcing is multiplicative and
119 thus depends on the state of the system itself, more sophisticated methodological treatments may
120 be needed. This may be achieved by a suitable change of variables before the analysis in order
121 to map the system to a process with additive noise [65], or explicitly monitoring the time series
122 for changing noise strengths [66]. Another controversial assumption when searching for imprints
123 of CSD to anticipate abrupt transitions is that the approach oversimplifies the dynamics of these
124 highly complex systems by approximating them with very low-dimensional models [67, 68]. This
125 valid concern should be addressed in each specific case. In many complex systems, however, the
126 relevant dynamics reduce to a low-dimensional manifold close to a critical transition [69, 70], and
127 hence, a low-dimensional dynamical-system approximation can be justified [71]. Moreover, close
128 to the critical point, the imprints of CSD will likely be detectable in different time series, encoding
129 the dynamics of different parts of the system under study.

130 False alarms, i.e., time series that show increases in the CSD indicators not related to nonlinear

131 feedbacks and the potential for a critical transition, are a crucial issue to address [72–74]. In gen-
132 eral, one does not expect to observe EWS in linear systems that are inherently monostable and do
133 not exhibit abrupt change. However, this does not mean that the presence of EWS can confidently
134 rule out such linear dynamics because the CSD indicators may increase for external reasons, e.g.,
135 related to changing characteristics of the driving noise [74]. The associated ‘prosecutor’s fallacy’
136 can arise when testing for EWS in a conditionally selected set of empirical time series apparently
137 exhibiting abrupt state transitions. This can lead to an undesired number of false positives and,
138 hence, to overconfidence in the skill of EWS [75]. The problem can be traced back to the fact that
139 *a priori*, a randomly selected time series would be much more likely to be produced by a linear
140 system without the potential for a critical transition (the blue area in Fig. 2). The risk of false
141 positives is therefore reduced if there are independent and strong reasons to assume that the system
142 under study may in principle undergo a critical transition, corresponding to a reduced prior proba-
143 bility of linear dynamics. As shown in Fig. 2, analyzing the EWS in a reduced set of time series
144 (the sum of green and purple areas) can effectively reduce the probability of false alarms compared
145 to the entire dataset (the sum of blue and purple areas). Moreover, the variance and the AC1 of the
146 noise-driven systems could increase for reasons unrelated to CSD, potentially giving false alarms
147 of a pending critical transition [64, 74]. To mitigate this source of false positives, more robust
148 indicators have recently been proposed [47, 55, 63]. These indicators estimate the linear restoring
149 rate directly under the assumption of autocorrelated noise with changing autocorrelation, and con-
150 firm that serially correlated non-stationary noise terms do not prevent the applicability of EWS in
151 general. Therefore, selecting a reduced set of time series and designing more specific indicators
152 are two promising approaches to reduce the probability of false-positive EWS.

153 In a practical setting, various sources of uncertainty must be considered before using the EWS
154 to predict an abrupt change. The weakening of negative, stabilizing feedbacks does not guaran-
155 tee strong positive feedbacks and alternative stable states. CSD analysis based on remote sensing
156 products obtained from merging signals from different sensors can lead to spurious results [74].
157 The statistical effects of gap filling and data preprocessing in the observational datasets must also
158 be considered [76, 77]. Other physical changes in a system may sometimes change its response
159 timescale, possibly leading to spurious EWS as well [78]. Additionally, false negatives may arise
160 due to the limitations of the theory, which is most accurate only in proximity to the bifurcation

161 point. For instance, sea ice is dominated by the growth-thickness feedback and becomes more
162 stable when its thickness decreases. The positive ice-albedo feedback only becomes relevant when
163 the area coverage changes substantially as well, but this may be too late to detect [78, 79]. More-
164 over, as we show in this work, the coupling between different subsystems can lead to false positive
165 or false negative EWS (see Box 3 below).

166 Consequently, analyzing EWS is valuable in systems where we know that there are strong pos-
167 itive feedbacks and, thus, the potential for critical transitions. In these situations, EWS analyses
168 can provide additional insight and predictability, such as the early detection of approaching tipping
169 points [33], quantitative measures of system resilience [58, 77], and the identification of emerg-
170 ing patterns of instability [56]. These capabilities lie beyond what can be obtained from merely
171 monitoring the mean state of a system or relying solely on employing comprehensive ESMs. Sta-
172 tistical rigour, e.g., assessing the statistical significance of increasing trends in CSD indicators, is
173 of course required, mainly to keep possible false alarms to a minimum. Using null models that
174 preserve both the variance and the autocorrelation structure in time series [37], for example, by
175 constructing phase surrogates [39, 40, 54, 55, 58, 76], is strongly recommended.

176 **OBSERVATIONAL EVIDENCE FOR DESTABILIZATION OF FOUR COUPLED TIPPING** 177 **ELEMENTS**

178 The dominant feedback mechanisms, and the CSD implied by them, mean that EWS are theo-
179 retically expected to precede a non-linear and abrupt change of the GrIS, the AMOC, the SAMS,
180 and the Amazon. This is further supported by paleoclimate proxy evidence and model simula-
181 tions [80]. This section will summarize recent observation-based results suggesting that these four
182 key tipping elements have been destabilizing over recent decades, and discuss the involved un-
183 certainties as well as the impacts of the physical couplings between these tipping elements on the
184 associated EWS.

Greenland ice sheet (GrIS)

For the GrIS (Fig. 3a), the potential for a critical transition comes mainly from the ice-albedo feedback and the melt-elevation feedback. The albedo feedback is mainly relevant in the context of the exposure of dark bare ice after the white snow layers have melted, while the atmospheric lapse rate causes the melt-elevation feedback: melting reduces the surface height, exposing the surface to increasing temperatures at lower elevations, leading to more melting. These feedbacks imply a critical surface temperature threshold beyond which stability of the current state of the GrIS is lost [81–84]. However, it also has been shown that – thanks to the inertia of the GrIS – this threshold can be temporarily exceeded without prompting a transition of the GrIS to an ice-free state [85]. As estimated from shallow ice cores, melt rates in central-western Greenland have accelerated substantially in the last decades. Rising variance and AC1 suggest that this part of the GrIS is approaching a critical transition. By fitting a conceptual model of the GrIS [82] to ice sheet height reconstructions based on these melt rates, it has been shown that the variance and AC1 increases match the theoretical result for a system approaching a critical transition [54]. Additionally, we demonstrate that the restoring rate λ in Fig. 3b, estimated under the assumption of non-stationary time-correlated noise, increases consistently with both the variance and AC1 (see Fig. 1d, e in ref. [54]), suggesting that these EWS are not false alarms caused by increasing serial correlations in the driving noise. However, the attribution of the detected CSD to the underlying feedback mechanisms remains uncertain, especially for the melt-elevation feedback, which operates on very slow time scales. The EWS are inconsistent with a linear response to rising temperatures, suggesting that at least the central-western part of the Greenland ice sheet has started to destabilize. Interestingly, model simulations have identified this region as particularly important for the stability of the entire GrIS [86]. Precipitation rates over Greenland are projected to increase due to warmer air temperatures, but to what degree this will counteract the albedo and melt-elevation feedbacks is currently an open question [83, 87, 88]. Negative feedbacks may slow the ablation of the GrIS once critical forcing levels are crossed, and may even lead to alternative stable GrIS states at lower elevations [89]. For example, increasing precipitation with decreasing GrIS height can explain how a smaller GrIS persisted during the last (Eemian) interglacial, despite it being regionally warmer than the Holocene [90, 91]. Additionally, the glacial isostatic adjust-

214 ment after initial ice loss might counteract the positive feedbacks to some extent and stabilize the
215 GrIS [85, 86, 92].

216 **Atlantic Meridional Overturning Circulation (AMOC)**

217 For the AMOC (Fig. 3c), the nonlinearity that leads to bi-stability and, thus, the potential for an
218 abrupt transition is dominated by the salt-advection feedback [93]. Paleoclimate proxy evidence
219 confirms that the AMOC has relatively abruptly switched between the current strong circulation
220 mode and a substantially weaker one [94]. While recent work has shown a clear AMOC saddle-
221 node bifurcation in a complex climate model [52, 95], some comprehensive climate models con-
222 tinue to have difficulties reproducing the AMOC's bistability, and a recent model intercomparison
223 has highlighted the importance of the strength of the AMOC after weakening and the response of
224 deep convection to the system's bistability [96]. The salt-advection feedback is expected to become
225 increasingly relevant as freshwater flux into the northern Atlantic increases due to enhanced GrIS
226 meltwater runoff [97], sea ice melting, and increased precipitation and runoff from the adjacent
227 continents due to an overall enhancing hydrological cycle in response to rising temperatures [98–
228 100]. Direct observations of AMOC strength indicate a decline in recent decades but are only
229 available since the early 2000s [101]. Therefore, several studies have used observational mea-
230 surements that date back further to calculate fingerprints of AMOC variability, for example, based
231 on sea-surface temperature (SST) and salinity measurements [102, 103]. These fingerprints are
232 verified by their (lagged) correlation with the AMOC streamfunction strength in comprehensive
233 climate models [102–104], and although the strength of this correlation varies in time and with the
234 strength of the forcing [103, 105], they may still be able to serve as a basis for identifying AMOC
235 stability changes. In fact, ref. [55] identified significant EWS in several independent SST- and
236 salinity-based AMOC fingerprints. Recent work further confirms the presence and significance
237 of EWS in the North Atlantic, even when accounting for dataset uncertainties and non-stationary
238 observational coverage (see Fig. 3d in this study and Fig. 1 in ref. [76]). EWS have also been
239 found in paleoclimate-based reconstructions of the Atlantic Multidecadal Variability [106]. These
240 results suggest that over the last century, the AMOC has evolved from relatively stable conditions
241 toward a state that is nearing a critical transition (Fig. 3d). Researchers have also attempted to use

242 these EWS to predict a time of collapse of the AMOC [107], but the uncertainties inherent in such
243 a prediction are too large for it to yield reliable estimates of potential tipping times [108].

244 **Amazon rainforest**

245 The Amazon rainforest is threatened by a combination of changing precipitation regimes and
246 drought patterns due to climate change on the one hand, and deforestation to make space for crop-
247 land and pasture on the other [109, 110]. Some climate models have simulated a relatively abrupt
248 dieback of the Amazon under emission scenarios with unmitigated global warming [111], others
249 simulate a more gradual response [112], yet others simulate clustered localized dieback [113], in-
250 dicating large uncertainty in model-based projections. Analysis of model simulations in which
251 Amazon dieback does occur suggests that the identification of CSD-based precursor signals in ad-
252 vance may be challenging because the modeled forcing is both relatively fast and exhibits changing
253 variability [45]. A determining factor for Amazon rainforest resilience, typically defined as the re-
254 turn rate from perturbations [114], is the amount of rainfall and its distribution over the year. Only
255 rainforest-type vegetation is stable under very high mean annual precipitation (MAP), whereas
256 savanna-type vegetation dominates for very low MAP. However, at intermediate values of MAP,
257 the vegetation system can be bistable, i.e., both vegetation types can coexist [115–117]. These
258 observation-based results suggest that single disturbances such as droughts or widespread fires can
259 trigger a transition from the rainforest to the low-tree-cover state within this bistable regime. More-
260 over, if—potentially in response to changing tropical Atlantic SST patterns, e.g., caused by AMOC
261 reductions—Amazon rainfall characteristics such as MAP, the dry-season length, or the amount of
262 dry-season rainfall, cross a threshold, the vegetation system could undergo a larger-scale critical
263 transition from the rainforest to the low-tree-cover state, in part due to the high level of local mois-
264 ture recycling in the Amazon. Rainforest resilience, measured in terms of the AC1 coefficient
265 estimated from remotely sensed vegetation data, is lower in regions with lower MAP [118, 119],
266 especially in those regions with high inter-annual precipitation variability [119]. Furthermore,
267 recent results based on different remotely sensed vegetation indices show widespread loss of re-
268 silience since the early 2000s, with faster resilience loss in regions with lower MAP and in areas
269 closer to human land use activity [56, 58]. Since the main focus is on results based on merged Veg-

270 etation Optical Depth (VOD) data, these results could be biased [74]. However, the resilience loss
271 has recently been confirmed by a comparison of resilience indicators applied to four single-sensor
272 VOD datasets [120], as well as using single-sensor optical remote sensing data [77]. We confirm
273 these results here by observing increases in λ (Fig. 3f) of the merged VOD and two single-sensor
274 VOD datasets averaged over the Amazon basin. This serves as a cross-check of the previously
275 reported increasing variance and AC1 [56, 58].

276 **South American monsoon system (SAMS)**

277 Deforestation and degradation of the Amazon rainforest pose arguably the greatest threat to the
278 ecosystem [109]. Due to the lower evapotranspiration rates of cropland and pasture compared to
279 rainforest, deforestation and, more generally, forest degradation and local transitions from rain-
280 forest to savanna reduce the moisture that is fed back to the easterly low-level flow across the
281 Amazon basin. This recycled moisture is key to a positive feedback between convective latent
282 heating over the Amazon and the low-level inflow of moist air from the tropical Atlantic Ocean.
283 A deforestation-induced breakdown of this feedback could lead to a state shift of the South Amer-
284 ican Monsoon circulation and hence to abrupt and substantial rainfall reductions in the western
285 Amazon and further downstream toward subtropical South America [121]. Using time series of
286 monthly rainfall rates in the western Amazon (Fig. 3g), CSD in terms of rising variance and AC1
287 can be detected [57]. We show here that λ increases consistently with the other two indicators
288 (compare Fig. 3h to Fig. 6c, d in ref. [57]). Simulations with a nonlinear model of the atmo-
289 spheric moisture transport and its interactions with the Amazon rainforest show that these EWS
290 are consistent with approaching the breakdown of the feedback between latent heating and mois-
291 ture inflow to the Amazon basin [57]. Moreover, a collapse of this positive feedback should be
292 preceded by an increasing dry-season length, which has been reported for large parts of the Ama-
293 zon [122, 123]. Although the Amazon rainforest and SAMS are tightly coupled, we treat them as
294 two distinct tipping elements due to the differing origins and dynamics of their respective instabili-
295 ties. We thus have observational evidence that, in addition to the Amazon vegetation system itself,
296 the coupled vegetation-atmosphere system in tropical South America is destabilizing consistently
297 with an approaching tipping point.

298 **Uncertainties and effect of coupling on critical temperature levels**

299 The four tipping elements considered here are strongly coupled, and these interactions can
300 lead to nonlinear responses in each system. (see Box 2 and ref. [11]). These couplings alter the
301 critical temperature levels at which transitions are expected and, as we show in Box 3, can cause
302 misleading false positive or false negative EWS.

303 The physical couplings remain challenging to represent accurately in state-of-the-art ESMs,
304 which is one of the reasons why their projections remain uncertain in their estimates of the critical
305 thresholds of suggested tipping elements [26, 124, 125]. Hence, ESMs alone are not currently reli-
306 able for estimating critical temperature forcing levels. Complementarily, observational approaches
307 based on CSD are founded on the theory that the critical point is associated with diverging vari-
308 ance, $AC1 = 1$, and the restoring rate λ reaching zero from below. In principle, this can be used to
309 estimate critical forcing levels [54, 125]. In practice, however, the available observational records,
310 covering time spans from decades to, at most, a few centuries, are in most cases too short and too
311 uncertain to constrain the dynamics of the tipping elements in question to a degree that would allow
312 for reliable estimates of the critical forcing levels [108]. Furthermore, extrapolating the values of
313 the different CSD indicators may ignore other possibly important factors such as the interactions
314 among Earth system components (see the third model in Box 3). For example, uncertainties in our
315 estimates of the speed at which one tipping element changes will directly propagate, generally in a
316 nonlinear way, adding to uncertainties for the critical thresholds of other tipping elements that are
317 coupled to it [126]. Moreover, noise-induced effects can, in practice, cause the transition to occur
318 long before the critical value is reached (see the fourth model in Box 3).

319 **OUTLOOK AND STIMULI FOR FURTHER RESEARCH**

320 Critical transitions of the four Earth system tipping elements considered here would have dra-
321 matic ecological and socioeconomic consequences on a global scale [3]. Therefore, it is vital to
322 estimate the critical temperature levels at which the state transitions are expected. So far, estimates
323 given in the literature are mainly based on expert knowledge [127] and different model experiments
324 that are difficult to compare [124, 125]. Given existing shortcomings, we encourage researchers

325 across scientific disciplines to develop more sophisticated methods to estimate critical forcing lev-
326 els and to anticipate the associated transitions. Promising advances have, for example, been made
327 using transfer operator approaches [128]. The exploding application of machine learning in the
328 natural sciences also promises advances for predicting abrupt transitions. Recent work shows that
329 a deep learning approach can pick up informative changes in time-series data in addition to CSD-
330 based indicators [129–131]. However, EWS should only be searched for in situations where there
331 are, *a priori* and independently from the EWS analysis, good reasons to assume that a critical
332 transition may occur. For the Earth system components we investigated here, this is the case. An
333 important requirement for time-series-based methods to anticipate abrupt transitions, such as the
334 CSD-based EWS, is that they should be applicable to observations. This implies that methods that
335 need large amounts of data, as would typically only arise from simulations, would be less useful
336 in practice.

337 Given the respective caveats with approaches that are either entirely based on ESMs or entirely
338 on statistical EWS, combining these complementary approaches presents an important subject for
339 future research. One promising strategy, illustrated in Fig. S1, involves using observation-based
340 EWS to constrain or assign weights to models according to their capability of reproducing indi-
341 cations of CSD found in corresponding observations. The simulations confined in this way (red
342 line in Fig. S1) would have a lower spread in future projections. Ideally, these model constraints
343 should be done in a way that points toward shortcomings in the model equations and would thus
344 directly help to improve the model mechanics with regard to the relevant feedbacks. It should be
345 noted, however, that the spread across models can be too large for this to work, as is the case for
346 AMOC stability in CMIP6 models [132].

347 **Toward a global early warning system**

348 With ongoing global warming, and in particular because Arctic temperatures are rising much
349 faster than the global average, the risk increases that the GrIS and the AMOC may undergo critical
350 transitions in the near future [2]. A transition of the AMOC would, in turn, lead to changing
351 rainfall patterns in tropical South America, with uncertain consequences for the Amazon and the
352 South American monsoon.

353 Given the summarized findings, instituting a tipping element monitoring and warning system
354 could pay huge societal dividends, both as an aid to adaptation and a potential trigger of accelerated
355 mitigation action. Such a system would record the temporal variability of the coupled Earth system
356 components discussed here, as well as other potentially unstable parts of the Earth system, such
357 as the West Antarctic Ice Sheet, boreal forests, or the Asian monsoon systems. High-resolution,
358 spatially homogeneously distributed data for the melt process of the GrIS, the variability of the
359 AMOC, and the vegetation of the Amazon ecosystem are required for such a monitoring system.
360 Remotely sensed data products will play an important role in this context, but longer-term recon-
361 structions are also crucial to cover the relevant time scales. How many years of observations are
362 needed to reliably detect EWS depends on the specific dynamics and natural variability of each
363 system. Incorporating suitable machine learning approaches will likely be helpful to continuously
364 search for emerging signs of destabilization. Such a comprehensive global warning system, inte-
365 grating advanced observational techniques and model improvements, will provide the information
366 needed for timely interventions to mitigate the profound ecological and socio-economic impacts
367 of crossing critical climate thresholds.

368 **BOX 1**

369 **Theory: Critical slowing down and early-warning signals**

370 In the climate system, tipping points usually refer to thresholds in forcing or control parameters
371 at which a small additional perturbation can trigger a large-scale, abrupt change, often taking
372 place over a few decades or less [133]. These rapid changes typically involve shifts from one
373 equilibrium state to another, explained by classical bifurcation theory for autonomous dynamical
374 systems. When extended to non-autonomous systems (i.e., systems affected by time-dependent
375 forcing), bifurcations are one of several types of tipping identified [134], with the other two being
376 noise-induced tipping and rate-induced tipping [135].

377 *Mathematical derivation.* The concept of CSD prior to a bifurcation-induced abrupt transition
378 and the statistical EWS implied by CSD can be understood as follows. Consider a general random
379 dynamical system of the form,

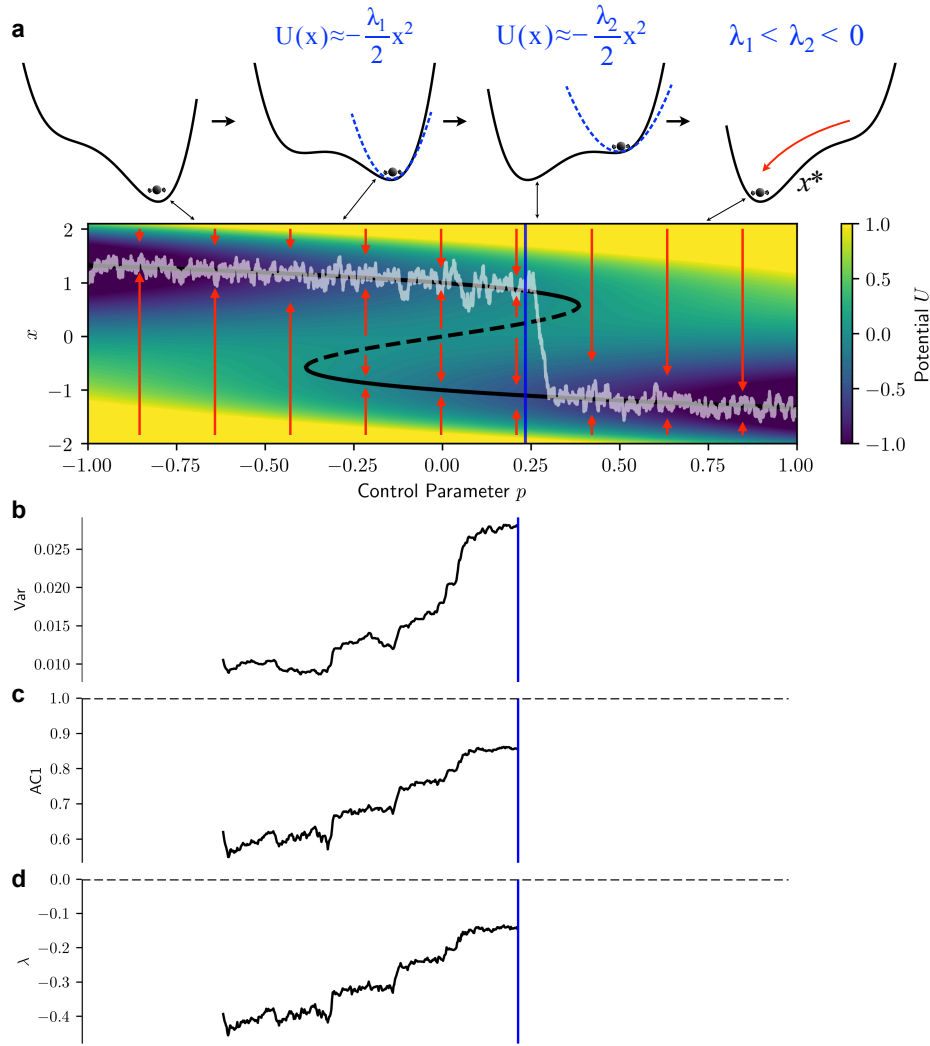
$$\frac{d}{dt}x(t) = -U'(x) + \eta(t) \quad (1)$$

380 for a state variable x , a nonlinear potential function U , and additive white noise η with standard
381 deviation σ . Assume that this system has a stable fixed point (i.e., an equilibrium state) x^* around
382 which the fast time scale dynamics occur. Near the fixed point, i.e., for x near x^* , the potential
383 U can be approximated by a quadratic function, $U(x) \approx -\lambda x^2/2$ with the parameter $\lambda < 0$. As
384 shown in Fig. B1, the potential well becomes less steep as λ approaches 0, indicating weaker
385 restoring forces and reduced stability of the fixed point.

386 Approximating the potential by a quadratic function corresponds to a linearization of the equa-
387 tion of motion around x^* . For the fluctuations $\Delta x = x - x^*$, one can obtain analytical formulae
388 of their statistical properties. The variance of these fluctuations is given by $\text{Var}(\Delta x) = -\sigma^2/2\lambda$
389 and their lag-1 autocorrelation (AC1) at sampling time step Δt is $\text{AC1} = e^{\lambda\Delta t}$. Hence, if the fixed
390 point loses stability and thus λ approaches zero from below, both the variance and the lag-one
391 autocorrelation will increase. Increases in variance and AC1 are the classical indicators of CSD:
392 The system responds ever more slowly to the noise perturbations, reflected by rising variance and
393 AC1. These can thus serve as EWS for a forthcoming critical transition. The above relationships
394 between variance and autocorrelation on the one hand, and the recovery rate λ estimated via re-

coveries from large perturbations, on the other hand, have recently been confirmed in remotely sensed vegetation data at a global scale [58, 77]. The empirical manifestation of the Fluctuation-Dissipation Theorem [136] shows that the proposed indicators can serve as stability measures not only for simple conceptual model systems but also for complex real-world systems. Recent research has broadened the scope of CSD-based methodology. For instance, Boettner et al. [63] consider a generalized auto-regression model as the basis for CSD analysis, and Morr et al. [47] employ model-fitting methods based on observed power spectra and correlation structures. These approaches pertain particularly to systems forced by a red noise term η , a type of correlated noise that is much more realistic in natural systems than white noise.

In physical terms, as a state transition is approached, the negative feedback that maintains (dynamical) stability becomes weaker relative to the positive feedback that takes over at the bifurcation point and propels the transition [137]. A slowing recovery from perturbations is the direct manifestation of the weakening negative feedback. EWS can thus be seen as quantifying this changing balance of feedbacks.



409 **Fig. B1. Schematic illustrating CSD and the associated EWS in a conceptual tipping system.**
 410 (a) The system in a double-well potential driven by additive white noise. The bifurcation diagram
 411 is shown in black, with stable branches solid and the unstable branch dashed. The corresponding
 412 potential U is shown by the colors in the background and in the time slices above the figure. The
 413 direction of the feedback induced by this potential is indicated by the red arrows. An example time
 414 series is shown in white, and the blue vertical line indicates the empirically determined time point
 415 of the abrupt transition. Note that, due to the noise forcing the system, the transition occurs before
 416 the deterministic critical point is reached. (b-d) Increasing variance, AC1, and λ (following the
 417 method from ref. [55]), giving EWS for the forthcoming transition.

418 **BOX 2**

419 **Physical coupling between four climate tipping elements**

420 The four tipping elements we highlight are physically coupled and part of a larger network of
421 interacting tipping elements.

422 Amplified Arctic warming is contributing to accelerating GrIS melting. According to compre-
423 hensive model studies, the GrIS could eventually disappear after a critical temperature threshold
424 is crossed, with time scales ranging from centuries to millennia, depending on future warming
425 scenarios [81, 85]. Complete melting of the GrIS would lead to a global sea-level rise of more
426 than 7 m and could occur by the year 3000 AD under the RCP8.5 scenario [83]. Stable GrIS states
427 at intermediate heights may be possible due to higher accumulation rates at higher temperatures
428 and lower GrIS elevations, but even partial melting of the GrIS would already cause substantial
429 meltwater runoff [97]. This runoff would freshen the northern Atlantic and add to the freshen-
430 ing caused by sea ice melt and an enhanced hydrological cycle. This freshening, together with
431 further warming due to albedo reductions associated with Arctic sea-ice retreat, would make the
432 upper-level water masses in the northern Atlantic less dense and push the AMOC further toward
433 its critical threshold [138].

434 An AMOC collapse would have major impacts on the global climate system [99], particularly
435 on other potential tipping elements. The associated relative cooling of the North Atlantic would
436 likely have a stabilizing effect on the GrIS [100, 139]. However, the impact on the Amazon rainfor-
437 est and SAMS is more challenging to assess. A weakened or collapsed AMOC would reorganize
438 precipitation patterns across tropical South America by reshaping the meridional SST gradient in
439 the tropical Atlantic [139] and by driving a southward shift of the Intertropical Convergence Zone
440 (ITCZ) [140–142]. Both observations and model simulations suggest that the relationship between
441 SST anomalies in the northern and southern tropical Atlantic plays a key role in rainfall anomalies
442 in the Amazon [143]. Atlantic SST anomalies may be responsible for the two one-in-a-century
443 Amazon droughts of 2005 and 2010 [144]. Furthermore, six out of the seven most severe droughts
444 that occurred during the last four decades can be hindcasted from characteristic changes in tropical
445 Atlantic SST anomalies [145]. Additionally, AMOC weakening leaves excess heat in the tropi-

446 cal South Atlantic, enhancing convection there; this drives anomalous subsidence over the eastern
447 tropical Pacific, strengthens the Pacific trade winds, and intensifies the Walker circulation [146], a
448 key control on precipitation in tropical South America.

449 However, the specific impacts of an AMOC collapse on regional and seasonal precipitation pat-
450 terns in tropical South America remain uncertain. Early model results suggested that an AMOC
451 collapse would increase MAP over most parts of tropical South America [147]. In contrast, sub-
452 sequent simulations projected a marked decrease in MAP, mainly attributed to a weakening of the
453 monsoon, while the dry season could receive more rainfall [100, 148]. The observed relationships
454 between tropical Atlantic SSTs and rainfall amounts suggest, in combination with the AMOC col-
455 lapse pattern of cooling north of the equator and warming south of the equator, that such a collapse
456 might lead to an increase in Amazon rainfall especially in the dry season, thus possibly stabi-
457 lizing the Amazon rainforest [149, 150]. More recent simulations from multiple high-resolution
458 ESMs suggest that an AMOC collapse could lead to increased monsoon precipitation across South
459 America, especially in the southern Amazon [141]. Combining current vegetation distribution with
460 temperature and precipitation changes projected by these ESMs suggests that an AMOC collapse
461 would stabilize the Amazon forest, and even delay the critical regime shift of Amazon forests under
462 severe intensification of global warming cases [15]. Furthermore, paleoclimate evidence suggests
463 that during cold phases of the DO cycles, when the AMOC was likely in its weak mode, Amazon
464 rainfall was indeed higher than during the warm phases [151]. However, further model experi-
465 ments are needed to assess this interpretation of the employed speleothem proxies. Moreover, the
466 glacial climate boundary conditions, which appear to be necessary for DO cycles to occur, were
467 very different from today.

468 **BOX 3**

469 **Four types of misleading EWS induced by coupling**

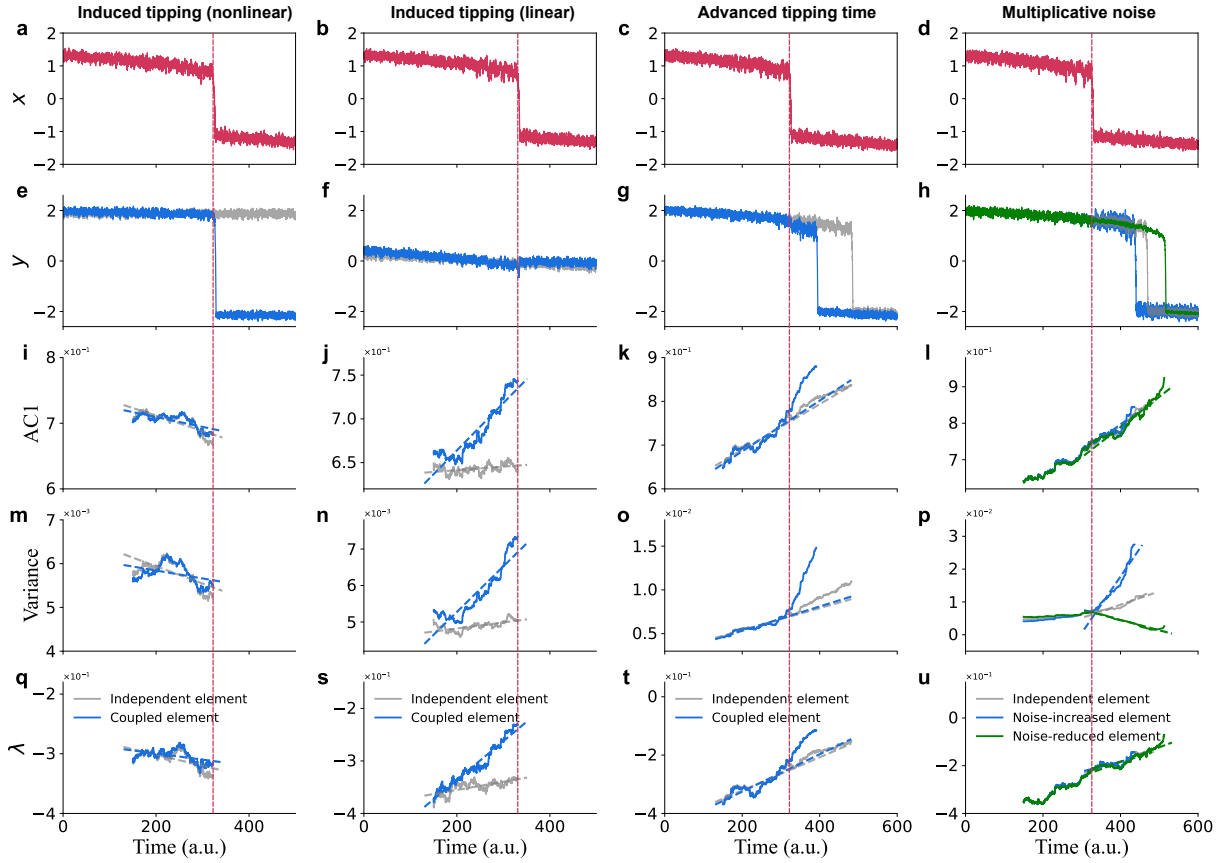
470 The presence of false-positive or false-negative EWS in coupled systems warrants more atten-
471 tion. Here, we present four conceptual cases that illustrate the occurrence of potentially misleading
472 EWS within a coupled system (Fig. B3). The coupled system consists of a leading element with
473 a saddle-node bifurcation (red line) and different following elements (blue or green line). An
474 independent following element (grey line) is also considered for comparison in each case.

475 (1) The abrupt change of the leading element induces the tipping of the following element
476 immediately through a large perturbation (see the first column of Fig. B3). As the collapse of the
477 following element is not related to a substantial loss of its own stability, the CSD-based parameters,
478 including AC1, variance, and λ , typically exhibit only weak or delayed EWS, driven indirectly by
479 the dynamics of the leading element, prior to the abrupt change in the coupled system [152].

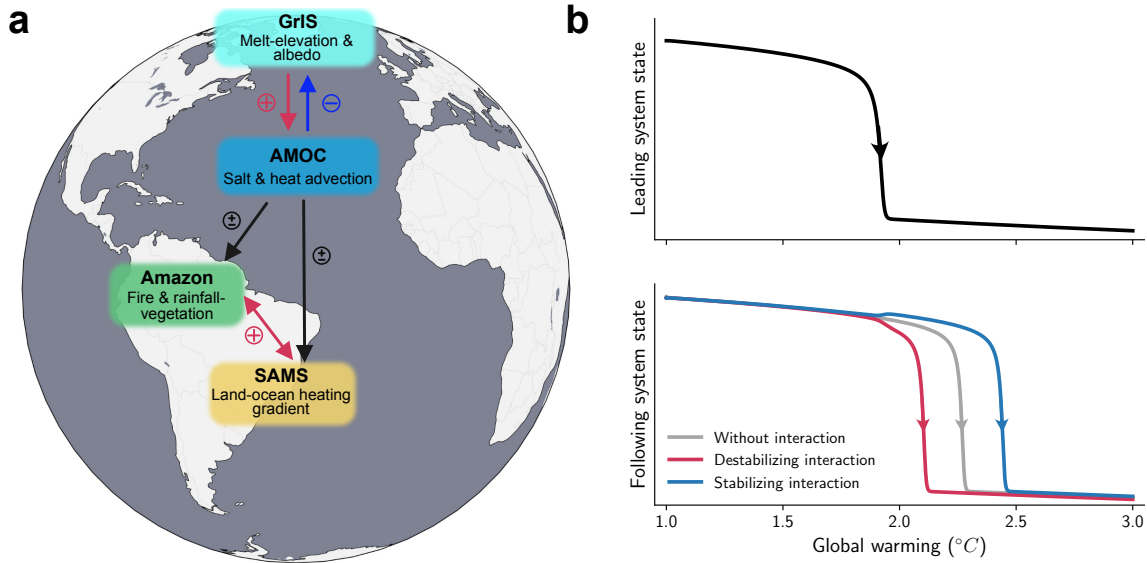
480 (2) The CSD from the leading element, transmitted through coupling as noise in the following
481 linear element, induces spurious EWS in the latter without any abrupt state change (see the second
482 column of Fig. B3). The signal of an increasing AC1, variance, and λ constitutes a false positive
483 alarm of tipping in the coupled element.

484 (3) The control parameter of the following element is dependent on the leading element, re-
485 sulting in an accelerated transition after the leading element's shift (see the third column of Fig.
486 B3). This acceleration invalidates the traditional approach of determining the time of an abrupt
487 transition by extrapolating current EWS signals, thus often leading to an underestimation of the
488 actual, now earlier, tipping time. This is reflected by the EWS of the coupled element deviating
489 significantly from the extrapolated values (dotted line) after the leading element's shift.

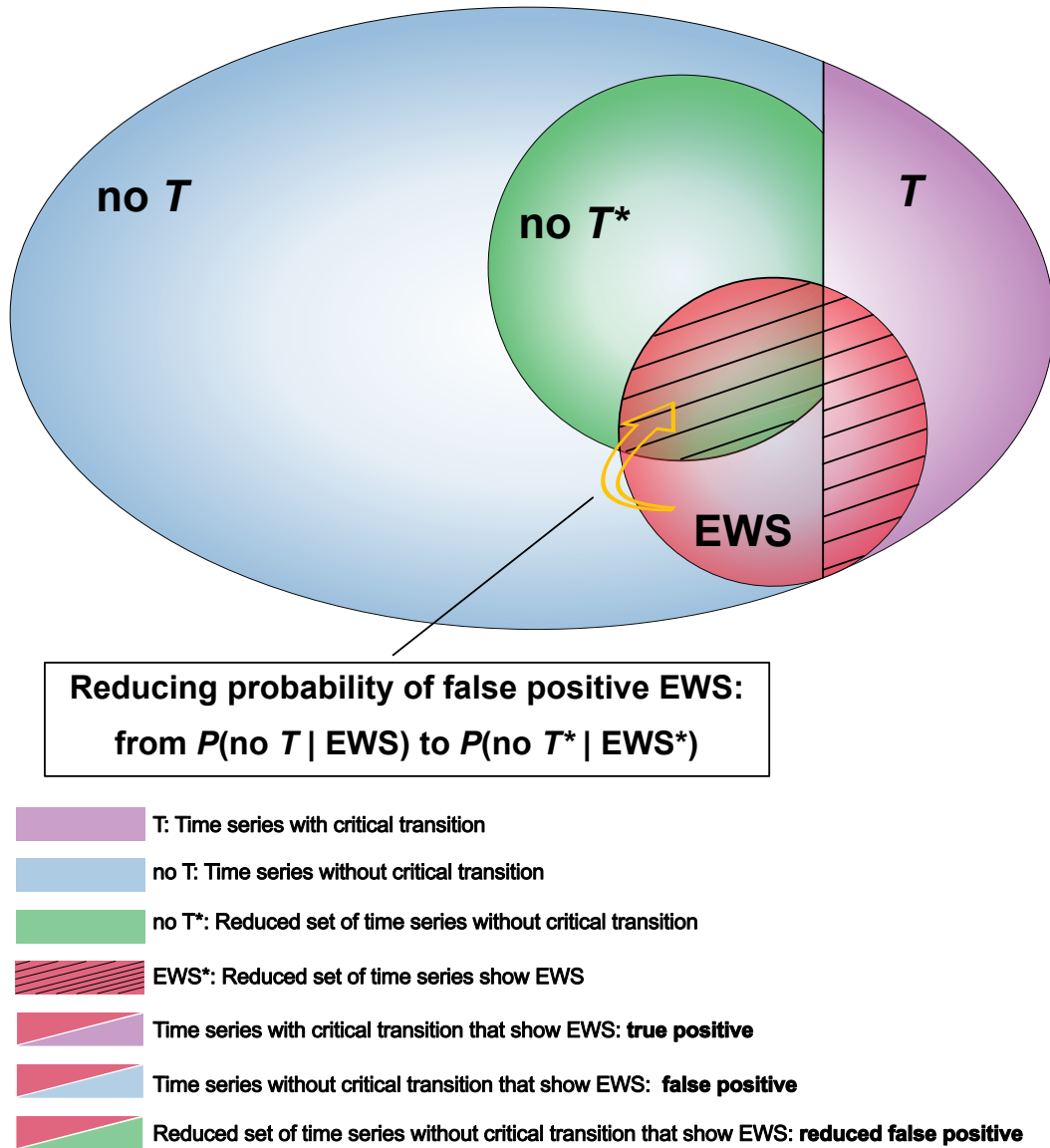
490 (4) The leading system's abrupt change increases (blue line) or decreases (green line) the noise
491 level of the following system, which advances (delays) the tipping time of the coupled element
492 (see the fourth column of Fig. B3). Under these conditions, neither the AC1 nor the restoring rate
493 λ is capable of detecting changes in the system's tipping time prompted by noise level variations.
494 Moreover, the trend in variance falsely indicates a stabilization of the coupled element when the
495 noise level is reduced (green line).



496 **Fig. B3. Four typical cases of false positive or negative EWS in coupled systems.** a-d, Sim-
 497 ulated time series of the leading system from a non-linear model driven by additive white noise.
 498 e-h, Simulated time series of the following systems, with independent elements (grey lines) and
 499 coupled elements (blue or green lines) following the same non-linear model (except for (f), which
 500 follows a linear model). In (e) and (f), the leading system is coupled as noise into the following
 501 system, while for (g) and (h), the parameters of the following system depend on the state of the
 502 leading system. i-l, ACI; m-l, Variance; and q-u, Restoring rate λ of the detrend time series shown
 503 in (e-h). Red vertical dotted lines indicate the time point of the abrupt transition for the leading ele-
 504 ment. The dotted lines represent the linear fits before (after) the leading element's abrupt transition
 505 for the first three (the fourth) scenarios. Specific model equations can be found in Methods.

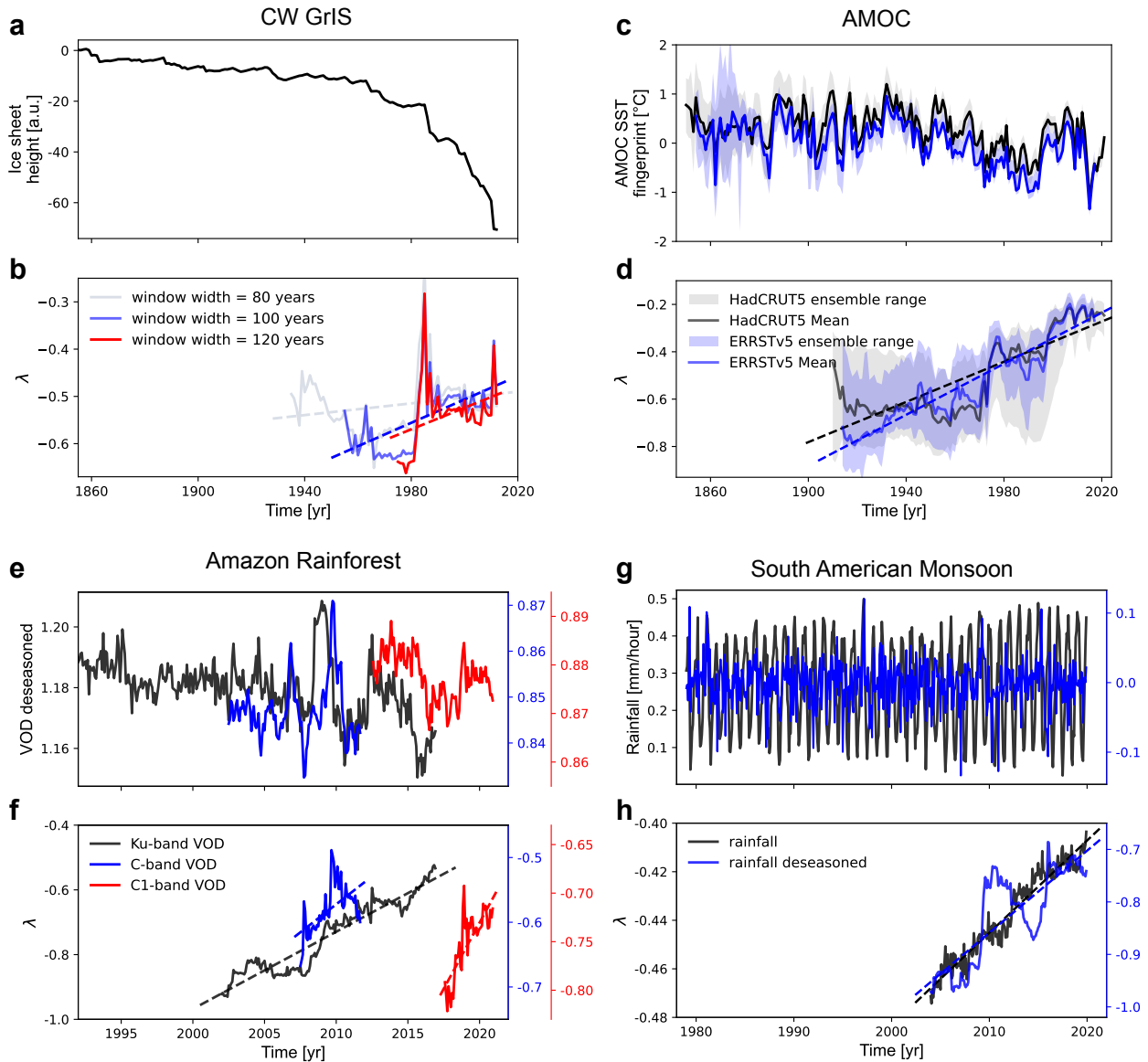


507 **Fig. 1. Schematic view of the four coupled tipping elements and comparison between cou-**
 508 **pled and independent tipping elements. a,** Map showing the geographical locations of the four
 509 tipping elements: GrIS, AMOC, Amazon, and SAMS. We list key reinforcing and, hence, po-
 510 tentially destabilizing feedbacks governing the dynamics of the different subsystems. Red (blue)
 511 arrows indicate destabilizing (stabilizing) effects from one tipping element on another, and black
 512 arrow indicates that the effect of an AMOC collapse on the Amazon and SAMS remains uncertain,
 513 although recent results suggest a stabilizing effect of AMOC weakening on the Amazon [15]. A
 514 stabilizing (destabilizing) effect of tipping element A on tipping element B is present if a transition
 515 of A raises (lowers) the critical threshold for a transition of B. **b,** Time series of system states ver-
 516 sus global warming for a conceptual model with coupled tipping elements. The system's forcing,
 517 here global warming, increases linearly with time. The y-axis represents an abstract system state
 518 variable used to illustrate qualitative shifts between stable states. The leading element (black line)
 519 and a following element (grey line) are characterized by two different double-well potentials with
 520 tipping points near 2 °C and 2.3 °C. The red and blue lines represent the state of two coupled fol-
 521 lowing elements, whose control parameters depend on the state of the leading element. The abrupt
 522 state transition of the leading element destabilizes (red line) or stabilizes (blue line) the following
 523 system, shifting its tipping threshold below or above 2.3 °C.



524 **Fig. 2. Schematic illustrating the role of false positive EWS and how to reduce their prob-**
 525 **ability.** The set of all available time series is first separated into the subset that exhibit a criti-
 526 cal (bifurcation-induced) transition (“T”, purple) and those without (“no T”, blue). The set ex-
 527 hibiting EWS (red) covers parts of both; the overlap with the set “T” corresponds to true posi-
 528 tive EWS, the overlap with “no T” corresponds to false positives, and the part of “T” not over-
 529 lapping with EWS corresponds to false negatives. The probability of false positives, given by
 530 $P(\text{no } T \mid \text{EWS}) = P(\text{no } T \cap \text{EWS})/P(\text{EWS})$, can be reduced by assuring *a priori* that there are

531 external reasons to assume that the time series under consideration may indeed undergo a critical
532 transition. This corresponds to restricting the set “no T” to the set “no T*” and for this restricted
533 set it holds that $P(\text{no T}^* \mid \text{EWS}^*) < P(\text{no T} \mid \text{EWS})$, where EWS* refers to the reduced set of
534 time series that exhibit EWS. Further reduction in false alarms can be achieved using more specific
535 CSD indicators, such as the restoring rate λ , estimated under non-stationary, time-correlated noise.



536 **Fig. 3. EWS for the central-western Greenland Ice Sheet (CW GrIS), the Atlantic Meridional**
 537 **Overturning Circulation (AMOC), the Amazon rainforest, and the South-American**
 538 **monsoon system (SAMS). a, Reconstructions of CW GrIS height changes at annual resolution**
 539 **from 1855 to 2013 [54]. c, Mean AMOC fingerprint index (black line) and min-max range (grey**
 540 **area) of 200 uncertainty ensemble members for HadCRUT5 at annual resolution from 1850 to**
 541 **2022; Mean AMOC fingerprint index (blue line) and min-max range (purple area) of 1000 un-**
 542 **certainty ensemble members for ERRSTv5 at annual resolution from 1854 to 2017 [55, 76, 102].**
 543 **e, Monthly values of Ku-band Vegetation Optical Depth (VOD) deseasoned time series from the**

544 merged VODCA product from 1991 to 2017 (black line) [153]; Monthly values of C-band VOD
545 deseasoned time series from the AMSR-E sensor from 2002 to 2012 (blue line); Monthly values of
546 C1-band VOD deseasoned time series from the AMSR2 sensor from 2012 to 2021 (red line); All
547 three time series are averaged over those parts of the Amazon basin that have a broadleaf fraction
548 above 80% [56]. **g**, Monthly rainfall rates in the western Amazon from 1979 to 2020, averaged
549 over the region defined by 4°S-12.5°S and 62.5°W-72.5°W [57]. Deseasoned versions of time se-
550 ries are shown as blue lines. **b, d, f, h**, Restoring rate λ of the time series shown in (**a, c, e, g**).
551 λ is estimated by the method from ref. [55] with the assumption of non-stationary time-correlated
552 noise. Each time series is first nonlinearly detrended using a running mean. The λ values are then
553 estimated using sliding windows with the following widths: 80, 100, and 120 years for CW GrIS,
554 60 years for AMOC, 10 years for K-band VOD, 5 years for C-band and C1-band VOD, and 25
555 years for SAMS. Values are plotted at the end point of each window. All systems exhibit statisti-
556 cally significant EWS characterized by a positive trend (dashed lines) in λ . For details regarding
557 the data sources, detrending, statistical significance and robustness tests, we refer to the original
558 references [54, 56, 57, 76, 120].

559 **METHODS**

560 This section provides detailed information on the four coupled conceptual models shown in
 561 Box 3. The leading systems for Fig. B3 from a non-linear model with a saddle-node bifurcation:

$$\frac{dx}{dt} = -x^3 + x - \mu(t) + \eta(t), \quad (2)$$

562 where x is the system state, $\eta(t)$ is additive white noise with standard deviation $\sigma = 0.2$, and
 563 $\mu = -1 + 0.004t$ is the control parameter.

564 **A. Induced tipping (nonlinear)**

565 In a coupled system, the abrupt transition of the leading system may induce a direct large
 566 perturbation on the following system. This will cause it to tip immediately without any EWS. We
 567 introduced this scenario in the first column of the Fig. B3, and the equations of the following
 568 system (Fig. B3e) are:

$$\begin{cases} \frac{dy}{dt} = -0.5y^3 + 1.5y - \mu_0 + \eta(t) \\ \frac{dz}{dt} = -0.5z^3 + 1.5z - \nu(x) + \eta(t), \end{cases} \quad (3)$$

569 where y is the state of independent element with control parameter $\mu_0 = -0.5$; z is the state of
 570 coupled element with control parameter $\nu(x) = -\mu_0 - x = 0.5 - x$. It is worth noting that the
 571 control parameter of the independent element remains constant, meaning the system is in a stable
 572 potential and does not approach a bifurcation.

573 **B. Induced tipping (linear)**

574 The coupling among different components can transfer the CSD signal from one element near-
 575 ing a tipping point to another system that does not exhibit a tipping point itself. This may result in
 576 a false positive EWS, as the conventional CSD-based method cannot distinguish the signal's ori-
 577 gin and operates under the assumption of white noise. We introduced this scenario in the second
 578 column of Fig. B3. A linear model is employed here to represent the following system without a
 579 tipping point (Fig. B3f). The equations are:

$$\begin{cases} \frac{dy}{dt} = -4y - \mu(t) + \eta(t) \\ \frac{dz}{dt} = -4z - \nu(x) + \eta(t) \end{cases} \quad (4)$$

580 where y and z are the states of the independent element and coupled element, and $\nu(x) = \mu(t) +$
581 $2(|x| - 1)$ is the control parameter of the following element.

582 C. Advanced tipping time

583 When one system undergoes a transition, it can alter the background state of another system,
584 potentially inducing a transition in that second, following system as well. This change in back-
585 ground state is represented by the control parameter, where the second saddle-node bifurcation
586 system depends on the state of the leading system. The abrupt change in the leading system in-
587 creases the likelihood (i.e., earlier in our context) of the following system to tip, resulting in an
588 underestimation of the tipping time when based on the extrapolation of the available EWS. We
589 introduced this scenario in the third column of Fig. B3, and the equations of the following system
590 (Fig. B3g) are:

$$\begin{cases} \frac{dy}{dt} = -0.5y^3 + 1.5y - \mu(t) + \eta(t) \\ \frac{dz}{dt} = -0.5z^3 + 1.5z - \nu(x) + \eta(t) \end{cases} \quad (5)$$

591 where y and z are the states of the independent leading element and the coupled following element,
592 respectively. Moreover, $\nu(x) = \mu(t) + 0.2(1 - x)$ is the control parameter of following element.

593 D. Multiplicative noise

594 In a coupled system, the noise level of one system may be influenced by the state of another
595 system. A system with a high (or low) noise level will have a high (or low) probability of tipping
596 before reaching the deterministic bifurcation point, without significant changes in auto-correlation
597 or recovery rate. We introduced this scenario in the fourth column of Fig. B3, and the equations of
598 the following system (Fig. B3h) are:

$$\begin{cases} \frac{dy}{dt} = -0.5y^3 + 1.5y - \mu(t) + \eta(t) \\ \frac{dz}{dt} = -0.5z^3 + 1.5z - \mu(t) + \alpha(x) \cdot \eta(t) \end{cases} \quad (6)$$

599 where $\alpha(x) = 1 + 0.3(1 - x)$ represents the state of the leading system increasing the noise level
 600 in the following element, and $\alpha(x) = 1 - 0.3(1 - x)$ represents the state of the leading system,
 601 decreasing the noise level in the following system.

602 DATA AND CODE AVAILABILITY

603 All data presented here is publicly available. The Python code used to generate the figures,
 604 along with the associated data, is publicly available via GitHub at: [https://github.com/
 605 Tonny-liu/Four_tipping_elements](https://github.com/Tonny-liu/Four_tipping_elements).

606 ACKNOWLEDGEMENTS

607 NBoers and SB acknowledges funding by the Volkswagen Foundation. This is ClimTip con-
 608 tribution #12; the ClimTip project has received funding from the European Union’s Horizon Eu-
 609 rope research and innovation programme under grant agreement No. 101137601. This study
 610 received support from the European Space Agency Climate Change Initiative (ESA-CCI) Tipping
 611 Elements SIRENE project (contract no. 4000146954/24/I-LR). MBY and NBoers acknowledge
 612 funding by the European Union’s Horizon 2020 research and innovation programme under the
 613 Marie Skłodowska-Curie grant agreement No.956170. TLiu acknowledges funding from the Na-
 614 tional Key R&D Program of China No.2023YFE0109000. The work was supported by the UiT
 615 Aurora Centre Program, UiT The Arctic University of Norway (2020), and the Research Coun-
 616 cil of Norway (project number 314570). CAB and TML acknowledge funding from OptimESM
 617 which has received funding from the European Union’s Horizon Europe research and innovation
 618 programme under grant agreement No. 101081193. TS acknowledges support from the DFG
 619 STRIVE project (SM 710/2-1).

620 **AUTHOR CONTRIBUTIONS**

621 NBoers conceived and designed the study. NBoers and TLiu carried out the analyses with input
622 from SB, MBY, LB, NBochow, and AM. All authors discussed and interpreted the results. NBoers
623 and TLiu wrote the paper with input from all authors.

624 **ADDITIONAL INFORMATION**

625 Supplementary Information is available in the online version of the paper.

626 **COMPETING INTERESTS**

627 Authors declare no competing interests.

-
- 628 [1] Schellnhuber, H. J. Tipping elements in the Earth System. *Proceedings of the National Academy of*
629 *Sciences* **106**, 20561–20563 (2009).
- 630 [2] Schellnhuber, H. J., Rahmstorf, S. & Winkelmann, R. Why the right climate target was agreed in
631 Paris. *Nature Climate Change* **6**, 649–653 (2016).
- 632 [3] Lenton, T. M. *et al.* Climate tipping points—too risky to bet against. *Nature* **575**, 592–595 (2019).
- 633 [4] Dansgaard, W. *et al.* Evidence for general instability of past climate from a 250-kyr ice-core record.
634 *Nature* **364**, 218–220 (1993).
- 635 [5] Bond, G. *et al.* Persistent solar influence on North Atlantic climate during the Holocene. *Science*
636 **294**, 2130–2136 (2001).
- 637 [6] Crucifix, M. Pleistocene Glaciations. In *Climate Changes in the Holocene*, 77–106 (CRC Press,
638 2018).
- 639 [7] Peltier, W. R. & Vettoretti, G. Dansgaard-Oeschger oscillations predicted in a comprehensive model
640 of glacial climate: A “kicked” salt oscillator in the Atlantic. *Geophysical Research Letters* **41**, 7306–
641 7313 (2014).

- 642 [8] Drijfhout, S. *et al.* Catalogue of abrupt shifts in Intergovernmental Panel on Climate Change climate
643 models. *Proceedings of the National Academy of Sciences* **112**, E5777–E5786 (2015).
- 644 [9] Liu, W., Xie, S.-P., Liu, Z. & Zhu, J. Overlooked possibility of a collapsed Atlantic Meridional
645 Overturning Circulation in warming climate. *Science Advances* **3**, e1601666 (2017).
- 646 [10] Hopcroft, P. O. & Valdes, P. J. Paleoclimate-conditioning reveals a North Africa land–atmosphere
647 tipping point. *Proceedings of the National Academy of Sciences* **118**, e2108783118 (2021).
- 648 [11] Wunderling, N. *et al.* Climate tipping point interactions and cascades: a review. *Earth System*
649 *Dynamics* **15**, 41–74 (2024).
- 650 [12] Liu, T. *et al.* Teleconnections among tipping elements in the Earth system. *Nature Climate Change*
651 **13**, 67–74 (2023).
- 652 [13] Dekker, M. M., Von Der Heydt, A. S. & Dijkstra, H. A. Cascading transitions in the climate system.
653 *Earth System Dynamics* **9**, 1243–1260 (2018).
- 654 [14] Klose, A. K., Wunderling, N., Winkelmann, R. & Donges, J. F. What do we mean, ‘tipping cascade’?
655 *Environmental Research Letters* **16**, 125011 (2021).
- 656 [15] Nian, D. *et al.* A potential collapse of the Atlantic Meridional Overturning Circulation may stabilise
657 eastern Amazonian rainforests. *Communications Earth & Environment* **4**, 470 (2023).
- 658 [16] Ritchie, P. D., Clarke, J. J., Cox, P. M. & Huntingford, C. Overshooting tipping point thresholds in a
659 changing climate. *Nature* **592**, 517–523 (2021).
- 660 [17] Wunderling, N. *et al.* Global warming overshoots increase risks of climate tipping cascades in a
661 network model. *Nature Climate Change* **13**, 75–82 (2023).
- 662 [18] Cai, Y., Lenton, T. M. & Lontzek, T. S. Risk of multiple interacting tipping points should encourage
663 rapid CO₂ emission reduction. *Nature Climate Change* **6**, 520–525 (2016).
- 664 [19] Klockmann, M., Mikolajewicz, U., Kleppin, H. & Marotzke, J. Coupling of the subpolar gyre and
665 the overturning circulation during abrupt glacial climate transitions. *Geophysical Research Letters*
666 **47**, e2020GL090361 (2020).
- 667 [20] Meehl, G. A. *et al.* Context for interpreting equilibrium climate sensitivity and transient climate
668 response from the CMIP6 Earth system models. *Science Advances* **6**, eaba1981 (2020).
- 669 [21] Zelinka, M. D. *et al.* Causes of higher climate sensitivity in CMIP6 models. *Geophysical Research*
670 *Letters* **47**, e2019GL085782 (2020).

- 671 [22] Valdes, P. Built for stability. *Nature Geoscience* **4**, 414–416 (2011).
- 672 [23] Liu, W., Liu, Z. & Brady, E. C. Why is the AMOC monostable in coupled general circulation models?
673 *Journal of Climate* **27**, 2427–2443 (2014).
- 674 [24] Mecking, J., Drijfhout, S., Jackson, L. & Andrews, M. The effect of model bias on Atlantic freshwater
675 transport and implications for AMOC bi-stability. *Tellus A: Dynamic Meteorology and Oceanography*
676 **69**, 1299910 (2017).
- 677 [25] Weijer, W. *et al.* Stability of the Atlantic Meridional Overturning Circulation: A review and synthesis.
678 *Journal of Geophysical Research: Oceans* **124**, 5336–5375 (2019).
- 679 [26] McCarthy, G. D. & Caesar, L. Can we trust projections of amoc weakening based on climate models
680 that cannot reproduce the past? *Philosophical Transactions of the Royal Society A* **381**, 20220193
681 (2023).
- 682 [27] Thornalley, D. J. *et al.* Anomalously weak labrador sea convection and atlantic overturning during
683 the past 150 years. *Nature* **556**, 227–230 (2018).
- 684 [28] Caesar, L., McCarthy, G., Thornalley, D., Cahill, N. & Rahmstorf, S. Current Atlantic meridional
685 overturning circulation weakest in last millennium. *Nature Geoscience* **14**, 118–120 (2021).
- 686 [29] Kjeldsen, K. K. *et al.* Spatial and temporal distribution of mass loss from the Greenland Ice Sheet
687 since AD 1900. *Nature* **528**, 396–400 (2015).
- 688 [30] Smith, B. *et al.* Pervasive ice sheet mass loss reflects competing ocean and atmosphere processes.
689 *Science* **368**, 1239–1242 (2020).
- 690 [31] Held, H. & Kleinen, T. Detection of climate system bifurcations by degenerate fingerprinting. *Geo-*
691 *physical Research Letters* **31** (2004).
- 692 [32] Scheffer, M. *et al.* Early-warning signals for critical transitions. *Nature* **461**, 53–59 (2009).
- 693 [33] Lenton, T. M. Early warning of climate tipping points. *Nature climate change* **1**, 201–209 (2011).
- 694 [34] Armstrong McKay, D. I. & Lenton, T. M. Reduced carbon cycle resilience across the palaeocene–
695 eocene thermal maximum. *Climate of the Past* **14**, 1515–1527 (2018).
- 696 [35] Setty, S. *et al.* Loss of Earth system resilience during early Eocene transient global warming events.
697 *Science advances* **9**, eade5466 (2023).
- 698 [36] Boettner, C., Klinghammer, G., Boers, N., Westerhold, T. & Marwan, N. Early-warning signals for
699 Cenozoic climate transitions. *Quaternary Science Reviews* **270**, 107177 (2021).

- 700 [37] Dakos, V. *et al.* Slowing down as an early warning signal for abrupt climate change. *Proceedings of*
701 *the National Academy of Sciences* **105**, 14308–14312 (2008).
- 702 [38] Praetorius, S. K. & Mix, A. C. Synchronization of North Pacific and Greenland climates preceded
703 abrupt deglacial warming. *Science* **345**, 444–448 (2014).
- 704 [39] Rypdal, M. Early-warning signals for the onsets of Greenland interstadials and the Younger Dryas–
705 Preboreal transition. *Journal of Climate* **29**, 4047–4056 (2016).
- 706 [40] Boers, N. Early-warning signals for Dansgaard-Oeschger events in a high-resolution ice core record.
707 *Nature communications* **9**, 2556 (2018).
- 708 [41] Mitsui, T. & Boers, N. Statistical precursor signals for Dansgaard–Oeschger cooling transitions.
709 *Climate of the Past* **20**, 683–699 (2024).
- 710 [42] Carpenter, S. R. *et al.* Early warnings of regime shifts: a whole-ecosystem experiment. *Science* **332**,
711 1079–1082 (2011).
- 712 [43] Veraart, A. J. *et al.* Recovery rates reflect distance to a tipping point in a living system. *Nature* **481**,
713 357–359 (2012).
- 714 [44] Wang, R. *et al.* Flickering gives early warning signals of a critical transition to a eutrophic lake state.
715 *Nature* **492**, 419–422 (2012).
- 716 [45] Boulton, C. A., Good, P. & Lenton, T. M. Early warning signals of simulated Amazon rainforest
717 dieback. *Theoretical Ecology* **6**, 373–384 (2013).
- 718 [46] Trauth, M. H. *et al.* Early warning signals of the termination of the african humid period (s). *Nature*
719 *Communications* **15**, 3697 (2024).
- 720 [47] Morr, A. & Boers, N. Detection of Approaching Critical Transitions in Natural Systems Driven by
721 Red Noise. *Physical Review X* **14**, 021037 (2024).
- 722 [48] Lenton, T. M. *et al.* Using GENIE to study a tipping point in the climate system. *Philosophical*
723 *Transactions of the Royal Society A: Mathematical, Physical and Engineering Sciences* **367**, 871–
724 884 (2009).
- 725 [49] Boulton, C. A., Allison, L. C. & Lenton, T. M. Early warning signals of Atlantic Meridional Over-
726 turning Circulation collapse in a fully coupled climate model. *Nature communications* **5**, 5752 (2014).
- 727 [50] Klus, A., Prange, M., Varma, V. & Schulz, M. Spatial analysis of early-warning signals for a North
728 Atlantic climate transition in a coupled GCM. *Climate dynamics* **53**, 97–113 (2019).

- 729 [51] Rosier, S. H. *et al.* The tipping points and early warning indicators for Pine Island Glacier, West
730 Antarctica. *The Cryosphere* **15**, 1501–1516 (2021).
- 731 [52] van Westen, R. M., Kliphuis, M. & Dijkstra, H. A. Physics-based early warning signal shows that
732 AMOC is on tipping course. *Science advances* **10**, eadk1189 (2024).
- 733 [53] Boulton, C. A. & Lenton, T. M. Slowing down of North Pacific climate variability and its implications
734 for abrupt ecosystem change. *Proceedings of the National Academy of Sciences* **112**, 11496–11501
735 (2015).
- 736 [54] Boers, N. & Rypdal, M. Critical slowing down suggests that the western Greenland Ice Sheet is close
737 to a tipping point. *Proceedings of the National Academy of Sciences* **118**, e2024192118 (2021).
- 738 [55] Boers, N. Observation-based early-warning signals for a collapse of the Atlantic Meridional Over-
739 turning Circulation. *Nature Climate Change* **11**, 680–688 (2021).
- 740 [56] Boulton, C. A., Lenton, T. M. & Boers, N. Pronounced loss of amazon rainforest resilience since the
741 early 2000s. *Nature Climate Change* **12**, 271–278 (2022).
- 742 [57] Bochow, N. & Boers, N. The South American monsoon approaches a critical transition in response
743 to deforestation. *Science Advances* **9**, eadd9973 (2023).
- 744 [58] Smith, T., Traxl, D. & Boers, N. Empirical evidence for recent global shifts in vegetation resilience.
745 *Nature Climate Change* **12**, 477–484 (2022).
- 746 [59] Council, N. R. *et al.* *Abrupt impacts of climate change: Anticipating surprises* (National Academies
747 Press, 2013).
- 748 [60] Lenton, T. M. *et al.* Remotely sensing potential climate change tipping points across scales. *Nature*
749 *communications* **15**, 343 (2024).
- 750 [61] Rietkerk, M., Skiba, V., Weinans, E., Hébert, R. & Laepple, T. Ambiguity of early warning signals
751 for climate tipping points. *Nature Climate Change* 1–10 (2025).
- 752 [62] Ritchie, P. & Sieber, J. Early-warning indicators for rate-induced tipping. *Chaos: An Interdisciplinary*
753 *Journal of Nonlinear Science* **26** (2016).
- 754 [63] Boettner, C. & Boers, N. Critical slowing down in dynamical systems driven by nonstationary corre-
755 lated noise. *Physical Review Research* **4**, 013230 (2022).
- 756 [64] Clarke, J. J., Huntingford, C., Ritchie, P. D. & Cox, P. M. Seeking more robust early warning signals
757 for climate tipping points: the ratio of spectra method (ROSA). *Environmental Research Letters* **18**,

- 758 035006 (2023).
- 759 [65] Rubin, K. J., Pruessner, G. & Pavliotis, G. A. Mapping multiplicative to additive noise. *Journal of*
760 *Physics A: Mathematical and Theoretical* **47**, 195001 (2014).
- 761 [66] Morr, A., Riechers, K., Gorjão, L. R. & Boers, N. Anticipating critical transitions in multidimensional
762 systems driven by time-and state-dependent noise. *Physical Review Research* **6**, 033251 (2024).
- 763 [67] Bathiany, S. *et al.* Beyond bifurcation: using complex models to understand and predict abrupt
764 climate change. *Dynamics and Statistics of the Climate System* **1**, dzw004 (2016).
- 765 [68] Lucarini, V., Faranda, D. & Willeit, M. Bistable systems with stochastic noise: virtues and limits of
766 effective one-dimensional langevin equations. *Nonlinear Processes in Geophysics* **19**, 9–22 (2012).
- 767 [69] Trefois, C., Antony, P. M., Goncalves, J., Skupin, A. & Balling, R. Critical transitions in chronic
768 disease: transferring concepts from ecology to systems medicine. *Current opinion in biotechnology*
769 **34**, 48–55 (2015).
- 770 [70] Gao, J., Barzel, B. & Barabási, A.-L. Universal resilience patterns in complex networks. *Nature* **530**,
771 307–312 (2016).
- 772 [71] Thibeault, V., Allard, A. & Desrosiers, P. The low-rank hypothesis of complex systems. *Nature*
773 *Physics* 1–9 (2024).
- 774 [72] Kéfi, S., Dakos, V., Scheffer, M., Van Nes, E. H. & Rietkerk, M. Early warning signals also precede
775 non-catastrophic transitions. *Oikos* **122**, 641–648 (2013).
- 776 [73] Zimmerman, C., Wagner, T. J., Maroon, E. & McNamara, D. Slowed response of Atlantic merid-
777 ional overturning circulation not a robust signal of collapse. *Geophysical Research Letters* **52**,
778 e2024GL112415 (2025).
- 779 [74] Smith, T. *et al.* Reliability of resilience estimation based on multi-instrument time series. *Earth*
780 *System Dynamics* **14**, 173–183 (2023).
- 781 [75] Boettiger, C. & Hastings, A. Early warning signals and the prosecutor’s fallacy. *Proceedings of the*
782 *Royal Society B: Biological Sciences* **279**, 4734–4739 (2012).
- 783 [76] Ben-Yami, M., Skiba, V., Bathiany, S. & Boers, N. Uncertainties in critical slowing down indicators
784 of observation-based fingerprints of the Atlantic Overturning Circulation. *Nature Communications*
785 **14**, 8344 (2023).

- 786 [77] Smith, T. & Boers, N. Reliability of vegetation resilience estimates depends on biomass density.
787 *Nature Ecology & Evolution* **7**, 1799–1808 (2023).
- 788 [78] Wagner, T. J. & Eisenman, I. False alarms: How early warning signals falsely predict abrupt sea ice
789 loss. *Geophysical Research Letters* **42**, 10–333 (2015).
- 790 [79] Bathiany, S. *et al.* Statistical indicators of Arctic sea-ice stability—prospects and limitations. *The*
791 *Cryosphere* **10**, 1631–1645 (2016).
- 792 [80] Brovkin, V. *et al.* Past abrupt changes, tipping points and cascading impacts in the Earth system.
793 *Nature Geoscience* **14**, 550–558 (2021).
- 794 [81] Robinson, A., Calov, R. & Ganopolski, A. Multistability and critical thresholds of the Greenland ice
795 sheet. *Nature Climate Change* **2**, 429–432 (2012).
- 796 [82] Levermann, A. & Winkelmann, R. A simple equation for the melt elevation feedback of ice sheets.
797 *The Cryosphere* **10**, 1799–1807 (2016).
- 798 [83] Aschwanden, A. *et al.* Contribution of the Greenland Ice Sheet to sea level over the next millennium.
799 *Science advances* **5**, eaav9396 (2019).
- 800 [84] Pattyn, F. *et al.* The greenland and Antarctic ice sheets under 1.5 °C global warming. *Nature climate*
801 *change* **8**, 1053–1061 (2018).
- 802 [85] Bochow, N. *et al.* Overshooting the critical threshold for the Greenland ice sheet. *Nature* **622**, 528–
803 536 (2023).
- 804 [86] Petrini, M. *et al.* A topographically controlled tipping point for complete greenland ice sheet melt.
805 *The Cryosphere* **19**, 63–81 (2025).
- 806 [87] Hakuba, M. Z., Folini, D., Wild, M. & Schär, C. Impact of Greenland’s topographic height on
807 precipitation and snow accumulation in idealized simulations. *Journal of Geophysical Research:*
808 *Atmospheres* **117** (2012).
- 809 [88] Bochow, N., Poltronieri, A. & Boers, N. Projections of precipitation and temperatures in greenland
810 and the impact of spatially uniform anomalies on the evolution of the ice sheet. *The Cryosphere* **18**,
811 5825–5863 (2024).
- 812 [89] Gregory, J. M., George, S. E. & Smith, R. S. Large and irreversible future decline of the Greenland
813 ice sheet. *The Cryosphere* **14**, 4299–4322 (2020).

- 814 [90] NEEM community members. Eemian interglacial reconstructed from a Greenland folded ice core.
815 *Nature* **493**, 489–494 (2013).
- 816 [91] Colville, E. J. *et al.* Sr-Nd-Pb isotope evidence for ice-sheet presence on southern Greenland during
817 the Last Interglacial. *Science* **333**, 620–623 (2011).
- 818 [92] Zeitz, M., Haacker, J. M., Donges, J. F., Albrecht, T. & Winkelmann, R. Dynamic regimes of the
819 Greenland Ice sheet emerging from interacting melt–elevation and glacial isostatic adjustment feed-
820 backs. *Earth System Dynamics* **13**, 1077–1096 (2022).
- 821 [93] Stommel, H. Thermohaline Convection with Two Stable Regimes of Flow. *Tellus* **13**, 224–230
822 (1961).
- 823 [94] Henry, L. *et al.* North Atlantic ocean circulation and abrupt climate change during the last glaciation.
824 *Science* **353**, 470–474 (2016).
- 825 [95] van Westen, R. M., Vanderborcht, E. & Dijkstra, H. A. A saddle-node bifurcation is causing the
826 amoc collapse in the community earth system model. *EGUsphere [preprint]* **2025**, 1–29 (2025).
827 URL <https://doi.org/10.5194/egusphere-2025-14>.
- 828 [96] Jackson, L. C. *et al.* Understanding AMOC stability: the North Atlantic hosing model intercompari-
829 son project. *Geoscientific Model Development Discussions* **2022**, 1–32 (2022).
- 830 [97] Trusel, L. D. *et al.* Nonlinear rise in Greenland runoff in response to post-industrial Arctic warming.
831 *Nature* **564**, 104–108 (2018).
- 832 [98] Jackson, L. & Wood, R. Hysteresis and resilience of the AMOC in an eddy-permitting GCM. *Geo-
833 physical Research Letters* **45**, 8547–8556 (2018).
- 834 [99] Rahmstorf, S. Ocean circulation and climate during the past 120,000 years. *Nature* **419**, 207–214
835 (2002).
- 836 [100] Jackson, L. *et al.* Global and European climate impacts of a slowdown of the AMOC in a high
837 resolution GCM. *Climate dynamics* **45**, 3299–3316 (2015).
- 838 [101] Frajka-Williams, E. *et al.* Atlantic meridional overturning circulation: Observed transport and vari-
839 ability. *Frontiers in Marine Science* **6**, 260 (2019).
- 840 [102] Caesar, L., Rahmstorf, S., Robinson, A., Feulner, G. & Saba, V. Observed fingerprint of a weakening
841 Atlantic Ocean overturning circulation. *Nature* **556**, 191–196 (2018).

- 842 [103] Jackson, L. & Wood, R. Fingerprints for early detection of changes in the AMOC. *Journal of Climate*
843 **33**, 7027–7044 (2020).
- 844 [104] Zhu, C., Liu, Z., Zhang, S. & Wu, L. Likely accelerated weakening of Atlantic overturning circulation
845 emerges in optimal salinity fingerprint. *Nature Communications* **14**, 1245 (2023).
- 846 [105] Little, C. M., Zhao, M. & Buckley, M. W. Do surface temperature indices reflect centennial-timescale
847 trends in Atlantic meridional overturning circulation strength? *Geophysical Research Letters* **47**,
848 e2020GL090888 (2020).
- 849 [106] Michel, S. L. *et al.* Early warning signal for a tipping point suggested by a millennial Atlantic
850 Multidecadal Variability reconstruction. *Nature Communications* **13**, 5176 (2022).
- 851 [107] Ditlevsen, P. & Ditlevsen, S. Warning of a forthcoming collapse of the Atlantic meridional overturn-
852 ing circulation. *Nature Communications* **14**, 1–12 (2023).
- 853 [108] Ben-Yami, M., Morr, A., Bathiany, S. & Boers, N. Uncertainties too large to predict tipping times of
854 major Earth system components from historical data. *Science Advances* **10**, ead14841 (2024).
- 855 [109] Lovejoy, T. E. & Nobre, C. Amazon tipping point. *Science advances* **4**, eaat2340 (2018).
- 856 [110] Flores, B. M. *et al.* Critical transitions in the Amazon forest system. *Nature* **626**, 555–564 (2024).
- 857 [111] Cox, P. M. *et al.* Amazonian forest dieback under climate-carbon cycle projections for the 21st
858 century. *Theoretical and applied climatology* **78**, 137–156 (2004).
- 859 [112] Good, P., Jones, C., Lowe, J., Betts, R. & Gedney, N. Comparing tropical forest projections from
860 two generations of hadley centre earth system models, HadGEM2-ES and HadCM3LC. *Journal of*
861 *Climate* **26**, 495–511 (2013).
- 862 [113] Parry, I. M., Ritchie, P. D. & Cox, P. M. Evidence of localised Amazon rainforest dieback in CMIP6
863 models. *Earth System Dynamics* **13**, 1667–1675 (2022).
- 864 [114] Pimm, S. L. The complexity and stability of ecosystems. *Nature* **307**, 321–326 (1984).
- 865 [115] Hirota, M., Holmgren, M., Van Nes, E. H. & Scheffer, M. Global resilience of tropical forest and
866 savanna to critical transitions. *Science* **334**, 232–235 (2011).
- 867 [116] Wuyts, B., Champneys, A. R. & House, J. I. Amazonian forest-savanna bistability and human impact.
868 *Nature Communications* **8**, 15519 (2017).
- 869 [117] Ciemer, C. *et al.* Higher resilience to climatic disturbances in tropical vegetation exposed to more
870 variable rainfall. *Nature Geoscience* **12**, 174–179 (2019).

- 871 [118] Verbesselt, J. *et al.* Remotely sensed resilience of tropical forests. *Nature Climate Change* **6**, 1028–
872 1031 (2016).
- 873 [119] Smith, T. & Boers, N. Global vegetation resilience linked to water availability and variability. *Nature*
874 *Communications* **14**, 498 (2023).
- 875 [120] Blaschke, L. L. *et al.* Spatial correlation increase in single-sensor satellite data reveals loss of Amazon
876 rainforest resilience. *Earth's Future* **12**, e2023EF004040 (2024).
- 877 [121] Boers, N., Marwan, N., Barbosa, H. M. & Kurths, J. A deforestation-induced tipping point for the
878 South American monsoon system. *Scientific reports* **7**, 41489 (2017).
- 879 [122] Fu, R. *et al.* Increased dry-season length over southern Amazonia in recent decades and its implication
880 for future climate projection. *Proceedings of the National Academy of Sciences* **110**, 18110–18115
881 (2013).
- 882 [123] Leite-Filho, A. T., de Sousa Pontes, V. Y. & Costa, M. H. Effects of deforestation on the onset of the
883 rainy season and the duration of dry spells in southern Amazonia. *Journal of Geophysical Research:*
884 *Atmospheres* **124**, 5268–5281 (2019).
- 885 [124] Armstrong McKay, D. I. *et al.* Exceeding 1.5 °C global warming could trigger multiple climate
886 tipping points. *Science* **377**, eabn7950 (2022).
- 887 [125] Boers, N., Ghil, M. & Stocker, T. F. Theoretical and paleoclimatic evidence for abrupt transitions in
888 the Earth system. *Environmental Research Letters* **17**, 093006 (2022).
- 889 [126] Wunderling, N., Donges, J. F., Kurths, J. & Winkelmann, R. Interacting tipping elements increase
890 risk of climate domino effects under global warming. *Earth System Dynamics* **12**, 601–619 (2021).
- 891 [127] Kriegler, E., Hall, J. W., Held, H., Dawson, R. & Schellnhuber, H. J. Imprecise probability assessment
892 of tipping points in the climate system. *Proceedings of the national Academy of Sciences* **106**, 5041–
893 5046 (2009).
- 894 [128] Tantet, A., van der Burgt, F. R. & Dijkstra, H. A. An early warning indicator for atmospheric blocking
895 events using transfer operators. *Chaos: An Interdisciplinary Journal of Nonlinear Science* **25** (2015).
- 896 [129] Bury, T. M. *et al.* Deep learning for early warning signals of tipping points. *Proceedings of the*
897 *National Academy of Sciences* **118**, e2106140118 (2021).
- 898 [130] Bury, T. M. *et al.* Predicting discrete-time bifurcations with deep learning. *Nature Communications*
899 **14**, 6331 (2023).

- 900 [131] Huang, Y., Bathiany, S., Ashwin, P. & Boers, N. Deep learning for predicting rate-induced tipping.
901 *Nature Machine Intelligence* 1–10 (2024).
- 902 [132] Ben-Yami, M., Blaschke, L., Bathiany, S. & Boers, N. No critical slowing down in the Atlantic
903 Overturning Circulation in historical CMIP6 simulations. *EGUsphere [preprint]* **2024**, 1–38 (2024).
904 URL <https://doi.org/10.5194/egusphere-2024-1106>.
- 905 [133] Lee, J.-Y. *et al.* Future global climate: scenario-based projections and near-term information. In
906 *Climate change 2021: The physical science basis. Contribution of working group I to the sixth as-*
907 *essment report of the intergovernmental panel on climate change*, 553–672 (Cambridge University
908 Press, 2021).
- 909 [134] Ashwin, P., Wieczorek, S., Vitolo, R. & Cox, P. Tipping points in open systems: bifurcation, noise-
910 induced and rate-dependent examples in the climate system. *Philosophical Transactions of the Royal*
911 *Society A: Mathematical, Physical and Engineering Sciences* **370**, 1166–1184 (2012).
- 912 [135] Ritchie, P. D., Alkhayuon, H., Cox, P. M. & Wieczorek, S. Rate-induced tipping in natural and human
913 systems. *Earth System Dynamics* **14**, 669–683 (2023).
- 914 [136] Kubo, R. The fluctuation-dissipation theorem. *Reports on progress in physics* **29**, 255 (1966).
- 915 [137] Van Nes, E. H. *et al.* What do you mean, ‘tipping point’? *Trends in ecology & evolution* **31**, 902–904
916 (2016).
- 917 [138] Bakker, P. *et al.* Fate of the Atlantic Meridional Overturning Circulation: Strong decline under
918 continued warming and Greenland melting. *Geophysical Research Letters* **43**, 12–252 (2016).
- 919 [139] Liu, W., Fedorov, A. V., Xie, S.-P. & Hu, S. Climate impacts of a weakened Atlantic Meridional
920 Overturning Circulation in a warming climate. *Science advances* **6**, eaaz4876 (2020).
- 921 [140] Zhang, R. & Delworth, T. L. Simulated tropical response to a substantial weakening of the Atlantic
922 thermohaline circulation. *Journal of climate* **18**, 1853–1860 (2005).
- 923 [141] Ben-Yami, M. *et al.* Impacts of amoc collapse on monsoon rainfall: A multi-model comparison.
924 *Earth’s Future* **12**, e2023EF003959 (2024).
- 925 [142] Akabane, T. K. *et al.* Weaker atlantic overturning circulation increases the vulnerability of northern
926 amazon forests. *Nature Geoscience* 1–7 (2024).
- 927 [143] Yoon, J.-H. Multi-model analysis of the Atlantic influence on Southern Amazon rainfall. *Atmospheric*
928 *Science Letters* **17**, 122–127 (2016).

- 929 [144] Marengo, J. A., Tomasella, J., Alves, L. M., Soares, W. R. & Rodriguez, D. A. The drought of 2010
930 in the context of historical droughts in the Amazon region. *Geophysical research letters* **38** (2011).
- 931 [145] Ciemer, C. *et al.* An early-warning indicator for Amazon droughts exclusively based on tropical
932 Atlantic sea surface temperatures. *Environmental Research Letters* **15**, 094087 (2020).
- 933 [146] Orihuela-Pinto, B., England, M. H. & Taschetto, A. S. Interbasin and interhemispheric impacts of a
934 collapsed Atlantic Overturning Circulation. *Nature Climate Change* **12**, 558–565 (2022).
- 935 [147] Stouffer, R. J. *et al.* Investigating the causes of the response of the thermohaline circulation to past
936 and future climate changes. *Journal of climate* **19**, 1365–1387 (2006).
- 937 [148] Parsons, L. A., Yin, J., Overpeck, J. T., Stouffer, R. J. & Malyshev, S. Influence of the Atlantic
938 Meridional Overturning Circulation on the monsoon rainfall and carbon balance of the American
939 tropics. *Geophysical Research Letters* **41**, 146–151 (2014).
- 940 [149] Ciemer, C., Winkelmann, R., Kurths, J. & Boers, N. Impact of an AMOC weakening on the stability
941 of the southern Amazon rainforest. *The European Physical Journal Special Topics* **230**, 3065–3073
942 (2021).
- 943 [150] Good, P., Boers, N., Boulton, C. A., Lowe, J. A. & Richter, I. How might a collapse in the Atlantic
944 Meridional Overturning Circulation affect rainfall over tropical South America? *Climate Resilience
945 and Sustainability* **1**, e26 (2022).
- 946 [151] Mosblech, N. A. *et al.* North Atlantic forcing of Amazonian precipitation during the last ice age.
947 *Nature Geoscience* **5**, 817–820 (2012).
- 948 [152] Bathiany, S., Claussen, M. & Fraedrich, K. Detecting hotspots of atmosphere–vegetation interaction
949 via slowing down–Part 1: A stochastic approach. *Earth System Dynamics* **4**, 63–78 (2013).
- 950 [153] Moesinger, L. *et al.* The global long-term microwave vegetation optical depth climate archive
951 (VODCA). *Earth System Science Data* **12**, 177–196 (2020).